

Observation of Cooper minimum in krypton using high harmonic spectroscopy

A D Shiner¹, B E Schmidt², C Trallero-Herrero³, P B Corkum¹, J-C Kieffer², F Légaré² and D M Villeneuve¹

¹ Joint Attosecond Science Laboratory, National Research Council of Canada and University of Ottawa, 100 Sussex Drive, Ottawa, Ontario K1A 0R6, Canada

² INRS-Énergie et Matériaux, 1650 boul. Lionel-Boulet, C.P. 1020, Varennes (Québec) J3X 1S2, Canada

³ Department of Physics, Kansas State University, Manhattan, KS 66506, USA

E-mail: david.villeneuve@nrc.ca.

Received 16 September 2011, in final form 20 October 2011

Published 16 March 2012

Online at stacks.iop.org/JPhysB/45/074010

Abstract

High harmonic spectroscopy utilizes the methods of attosecond science to study electronic properties of atoms and molecules. We use a 1.8 μm 11 fs laser source to generate high harmonic spectra beyond 150 eV. The Cooper minimum in krypton is clearly visible in these spectra, and would otherwise be difficult to observe with 800 nm laser sources. We relate the shape of the spectrum to the photoionization cross section of krypton.

(Some figures in this article are in colour only in the electronic version)

High harmonic generation (HHG) can be described semi-classically as a three-step process [1, 2] in which an intense laser removes an electron from an atom or molecule, accelerates the electron, and then recombines the electron with the parent ion. The resulting emission extends to the extreme ultraviolet (XUV) and is composed of odd harmonics of the driving laser frequency. HHG provides a source of attosecond pulses [3–6]. The recombination of the recolliding electron also provides a measure of the electronic structure of molecules [7, 8]. Chemical reaction dynamics have been followed by using HHG as a probe [9, 10].

The cutoff frequency in HHG is given by [11] as $\Omega_{\text{max}} = 3.17U_p + I_p$, where $U_p = F^2/(4\omega^2)$ is the ponderomotive energy, F is the peak laser electric field, ω is the laser angular frequency, and I_p is the ionization potential (atomic units are used). U_p scales as $I\lambda^2$, where I is the peak laser intensity, and λ is the laser wavelength. To extend the cutoff frequency, it is advantageous to use a longer laser wavelength [12, 13]. On the negative side, the efficiency of the HHG process falls rapidly with increasing laser wavelength [14, 15].

High harmonic spectroscopy is a field of spectroscopy in which photorecombination cross sections (PRCSs) are measured by recording the HHG spectrum [16–18]. PRCSs are related to photoionization cross sections (PICSSs) through

a frequency-dependent prefactor [16, 19]. It has been shown that the PICSS can be accurately retrieved to 150 eV using high harmonic spectroscopy [8]. We show here that we can record a Cooper minimum in the photorecombination of krypton.

A Cooper minimum occurs in photoionization when the transition dipole matrix element falls to nearly zero [20], usually as a result of one photoionization partial wave transition moment changing sign while the other partial wave moments are small. The Cooper minimum has been clearly seen in argon [21–24] at 50 eV. The Cooper minimum in krypton is more difficult to detect because it is at a higher energy of 85 eV, and it is not as deep. In addition, due to krypton's low ionization potential, it is difficult to get the high harmonic spectrum to extend past 80 eV using 800 nm laser sources. Using a novel laser source, we resolve the krypton Cooper minimum in HHG.

Experiments were performed at the Advanced Laser Light Source (ALLS) at INRS-EMT. The laser source for the HHG experiment is based on frequency conversion from the Ti:Sa wavelength of 800 nm to 1.8 μm with commercial optical parametric amplifier (OPA) technology followed by subsequent pulse compression. A Ti:Sa amplifier delivers 45 fs pulses with 6 mJ pulse energy at a repetition rate of 100 Hz. Frequency conversion to the IR spectral range is

achieved by utilizing the idler out of a fluorescence seeded high energy OPA (HE TOPAS, Light Conversion). It provides 52 fs pulses with pulse energy of 950 μJ which are focused into an argon-filled hollow-core fibre (HCF) by a $f = 1$ m lens made of CaF_2 . Pulse shortening is achieved with nonlinear propagation in the HCF and linear propagation through bulk material in the anomalous dispersion regime [25]. Self-phase modulation (SPM) in the 1 m long fibre is the main driving source for spectral broadening of the initial OPA spectrum. After the fibre, the pulse duration is roughly that of the input pulse but its spectrum is significantly broadened. Collimation of the continuum is achieved with a mirror of 1 m focal length.

Self-steepening causes the spectral phase to become asymmetric, distinct from pure SPM which leads to the symmetric spectrum and phase. The symmetric part of the spectral phase is compensated afterwards by the negative group delay dispersion (GDD) introduced by the glass in the anomalous dispersion regime. Compared to other approaches [26–29], the glass compression scheme achieves the cancellation of the spectral phase-asymmetry arising from self-steepening during nonlinear propagation. It is balanced by the positive third order dispersion (TOD) of the glass. Thus, compression is not limited by the TOD of the bulk material which is always positive. A more detailed discussion and full numerical simulations of the propagation effects can be found in [30].

Several materials contribute to the pulse propagation after the fibre. CaF_2 windows on the HCF (1 mm thickness) and at the entrance of the high-harmonic chamber (3 mm thickness) have a minor effect because of very low dispersion. Compression mainly arises from the transmissive polarizer (nanoparticle polarizer, Thorlabs). Fine tuning is achieved by small tilts of the fused silica plate (2.0 mm thickness). Intensity control is achieved by rotating the half-wave plate in front of the HCF in combination with the polarizer located after the fibre. Pulse characterization is carried out with a home-built second harmonic generation frequency resolved optical gating (SHG-FROG) [31] setup designed for dispersion-free few-cycle pulse measurement [25]. This setup produces 11 fs pulses, corresponding to 1.8 optical cycles at 1.8 μm wavelength, with ~ 300 μJ pulse energy delivered to the HHG target chamber.

The gas jet in the HHG chamber (Parker pulsed valve) was operated with a constant backing pressure of ~ 3 bar of krypton. The gas density in the focus was estimated to be 10^{17} cm^{-3} . The thickness of the gas sample was 0.5 mm, in all cases much shorter than the Rayleigh range of the laser focus. The laser was focused ~ 2 mm before the gas jet to maximize phase matching for the short trajectories.

Harmonic radiation produced in the gas jet passed through a vertical slit with a 140 μm width into an XUV spectrometer where the beam was spectrally dispersed by a spherical grating (Shimadzu 30-002) and then imaged onto a microchannel plate (MCP) backed by a phosphor screen (Burle APD 3115 32/25/8 I EDR MgF2 P20). The resulting spectrum was recorded with a high dynamic range digital camera. In all cases, we averaged the observed spectra over many laser shots. The resulting harmonics propagated as a low divergence beam with

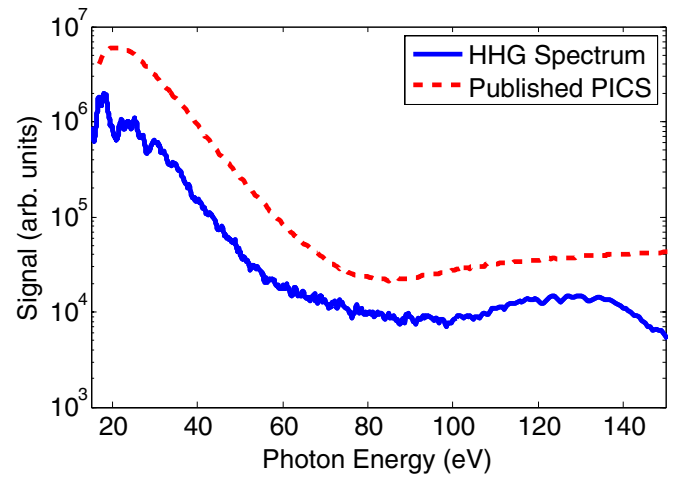


Figure 1. The blue curve shows the measured HHG spectrum from a Kr target. The raw spectrum $S(\lambda)$ has been converted from wavelength to frequency by multiplying by the Jacobian, i.e. $S(\Omega) = S(\lambda) d\lambda/d\Omega$. A minimum is evident around 90 eV. The dotted red curve shows the PICS for Kr [32]. The two curves are shifted vertically by an arbitrary amount in order to show them separately.

no visible annular structure, consistent with short trajectory only.

The HHG spectrum of Kr is shown in figure 1 for a laser intensity of 1.8×10^{14} W cm^{-2} . The spectrum extends beyond 150 eV. The raw spectrum from the XUV spectrometer has been corrected in the conversion from wavelength to frequency by multiplying by the Jacobian, i.e. $S(\Omega) = S(\lambda) d\lambda/d\Omega$. Also shown in the figure is the experimentally measured PICS [32] for Kr, showing a minimum around 85 eV.

The PRCS is related to the more common PICS by the relation [16, 19]

$$\frac{d^2\sigma^r}{\omega^2 d\Omega_n d\Omega_k} = \frac{d^2\sigma^i}{c^2 k^2 d\Omega_n d\Omega_k}. \quad (1)$$

Here, Ω_k is the solid angle of the emitted photoelectron, Ω_n is the solid angle of the photon polarization direction, and k is the final momentum of the photoelectron. In photoionization experiments, the outgoing electron direction is measured relative to the photon polarization direction as angle θ , and its anisotropy is characterized by the asymmetry parameter β , where $-1 < \beta < 2$. In HHG from atoms, the XUV is polarized parallel to the recolliding electron direction, so $\hat{n} \parallel \hat{k}$ and $\theta = 0$. The angle-resolved PICS is related to the angle-integrated cross section and the asymmetry parameter as follows [33]:

$$\frac{d\sigma^i}{d\Omega} = \frac{\sigma^i}{4\pi} [1 + \beta^i P_2(\cos(\theta))], \quad (2)$$

where $P_2(\cos(\theta)) \equiv \frac{3}{2} \cos^2(\theta) - \frac{1}{2}$. To compare our measured HHG spectra with previously published PICSs $\sigma^i(E)$ and asymmetry parameters $\beta^i(E)$, we use equation (2) to determine the $\theta = 0$ contribution.

We proceed to demonstrate that the observed minimum is a Cooper minimum [20]. A Cooper minimum occurs when the PICS goes through a minimum. The infrared laser will remove an electron from the 4p orbital; therefore,

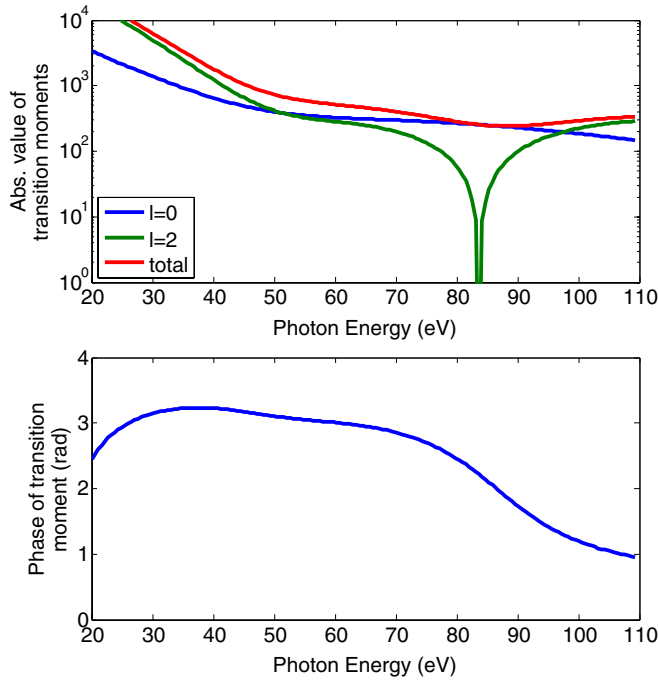


Figure 2. Top: the calculated absolute values of the transition dipoles for krypton for continuum wavefunction partial wave components $\ell = 0$ and $\ell = 2$. The total transition moment shows a minimum around 85 eV, which is caused by the $\ell = 2$ component going through a minimum at 83 eV. Bottom: the phase of the total transition moment as a function of photon energy. There is a gradual phase shift between 80 and 100 eV, showing the expected behaviour around a Cooper minimum.

the recombination will occur back to the 4p state. The Cooper minimum in argon around 50 eV is very prominent and has been extensively studied [21–24]. For both Ar and Kr, the continuum wavefunction associated with ionization from the p orbital will be composed of both s- and d-wave character. We first calculate the bound state 4p wavefunction using the procedure described by [21], which we summarize below.

The continuum wavefunction is calculated in three dimensions using an effective one-electron potential from the literature. Since the potential of the atomic ion is spherically symmetric, the electronic wavefunction is represented as a product of radial and angular components:

$$\psi_c(r, \theta, \phi) = \sum_{\ell m} \frac{1}{r} R_\ell(r) Y_\ell^m(\theta, \phi), \quad (3)$$

where R_ℓ is the radial wavefunction and Y_ℓ^m are spherical harmonics. The radial coordinate is treated numerically, whereas the two angular coordinates are treated analytically using angular momentum algebra. We use the independent particle model potential from [34] and include the centrifugal term for the reduced wave equation:

$$V_\ell(r) = \frac{\ell(\ell+1)}{2r^2} - \frac{1}{r} - \frac{Z-1}{H(e^{r/d}-1)+1} \quad (4)$$

with parameters $Z = 36$, $d = 0.617$, $H = 2.532$. The continuum functions are generated by numerically integrating the radial wave equation for a positive kinetic energy of the electron using the Numerov algorithm. To normalize the

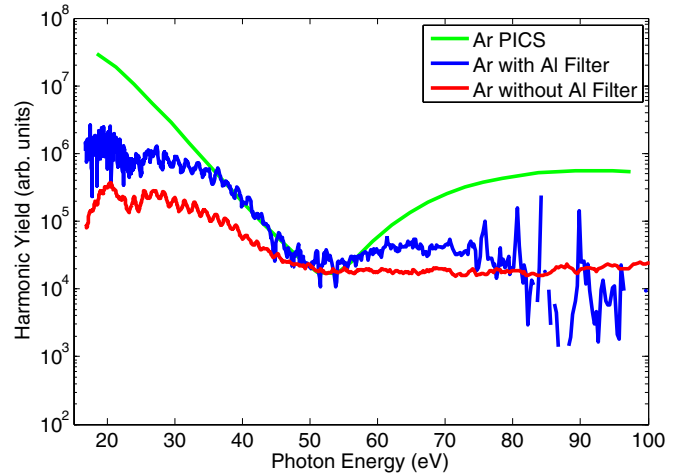


Figure 3. High harmonic spectra generated in argon. The red curve shows the spectrum recorded with the XUV spectrometer in the usual way. The Cooper minimum that is located around 50 eV is indistinct and has less contrast than previously seen. The lower contrast is due to higher frequency emission appearing at lower frequencies due to second order diffraction from the diffraction grating. When an aluminium filter is placed in the XUV beam (blue curve) with an L-shell absorption edge at 75 eV, the higher emission is cut, thereby increasing the contrast of the Cooper minimum and shifting it to 52 eV. The green curve shows the calculated PICS, from [21]. Note that the HHG spectrum shown in figure 1 was recorded with a different diffraction grating with reduced second order diffraction efficiency.

continuum wavefunctions, we match them asymptotically at large r using the formalism of Starace [33] for a potential composed of a short range potential plus a Coulomb tail.

The bound state wavefunction ψ_{4p} is calculated by GAMESS [35] using a correlation-corrected polarized triple zeta basis set (cc-pVTZ) for krypton. The photoionization dipole moment is given by

$$d = \langle \psi_{4p} | r | \psi_c \rangle \quad (5)$$

as a function of photon energy. Note that this model accounts for loss of electron kinetic energy from the Coulomb potential, by relating the photon energy Ω to the asymptotic electron kinetic energy E by $\Omega = E + I_p$, and therefore the ‘dispersion relation’ is self-consistent. Figure 2 shows the results of this calculation. The contribution to the total dipole moment from both angular momentum components is shown. The $\ell = 2$ partial wave component goes through zero near 83 eV, resulting in a gradual phase shift between 80 and 100 eV. The total dipole moment has a small minimum around 85 eV.

We now turn to the high harmonic spectrum of argon, shown in figure 3. The Cooper minimum in argon has been extensively studied in the context of high harmonic spectroscopy [21–24], so we do not need to revisit it in detail. The purpose of this section is to highlight a possible shortcoming of using a broad high harmonic spectrum. In particular, we show that the spectral content at higher energy can appear at lower energy due to second order diffraction of the diffraction grating used to disperse the spectrum. In most previous experiments, the second order diffraction is not an issue, because the HHG spectrum with 800 nm sources falls off

with increasing XUV photon energy. With near-infrared laser sources, particularly few-cycle sources, the HHG spectrum can be flat or even show a peak at a higher photon energy, which appears in second order in the low energy region of the spectrum.

Figure 3 shows the spectrum of argon recorded under similar conditions to krypton. The raw spectrum and one recorded with a 200 nm aluminium filter are shown. The aluminium filter has an L-edge at 75 eV that blocks emission above that energy. It can be seen that the spectrum with the aluminium filter (blue curve) clearly shows the presence of the Cooper minimum, whereas without the filter (red curve) the minimum has been filled in by energy from the 100 eV region of the spectrum by second order diffraction. We experienced a similar problem when recording the spectrum of xenon, due to the very strong emission around 100 eV which appeared as a second peak at 50 eV. This was improved when we replaced the Hitachi grating with a Shimadzu grating. The Shimadzu grating has a lower second order diffraction amplitude. All the spectra shown in this paper were recorded with the Shimadzu grating.

In conclusion, we have demonstrated that a 1.8 μm , 11 fs laser source can record a broad high harmonic spectrum in noble gases. These spectra contain features that reflect the PICS of the target, and in particular reveal the presence of Cooper minima. This work reinforces the current interpretation that HHG is a new form of spectroscopy that is sensitive to electronic properties of the valence shell of the target.

Acknowledgments

We gratefully acknowledge funding from Canada Foundation for Innovation (CFI), the Natural Sciences and Engineering Research Council of Canada (NSERC), Le Fonds Québécois de la Recherche sur la Nature et les Technologies (FQRNT), the Canadian Institute for Photonic Innovations (CIPI), and the National Research Council of Canada. We also thank François Poitras and Antoine Laramée for their support with the laser system.

References

- [1] Corkum P B 1993 *Phys. Rev. Lett.* **71** 1994
- [2] Schafer K J, Yang B, DiMauro L F and Kulander K C 1993 *Phys. Rev. Lett.* **70** 1599
- [3] Scrinzi A, Ivanov M Y, Kienberger R and Villeneuve D M 2006 *J. Phys. B: At. Mol. Opt. Phys.* **39** R1
- [4] Corkum P B and Krausz F 2007 *Nat. Phys.* **3** 381
- [5] Sansone G *et al* 2006 *Science* **314** 443
- [6] Chang Z and Corkum P B 2010 *J. Opt. Soc. Am. B* **27** B9
- [7] Itatani J, Levesque J, Zeidler D, Niikura H, Pépin H, Kieffer J C, Corkum P B and Villeneuve D M 2004 *Nature* **432** 867
- [8] Shiner A D, Schmidt B E, Trallero-Herrero C, Wörner H J, Patchkovskii S, Corkum P B, Kieffer J-C, Légaré F and Villeneuve D M 2011 *Nat. Phys.* **7** 464
- [9] Wörner H J, Bertrand J B, Kartashov D V, Corkum P B and Villeneuve D M 2010 *Nature* **466** 604
- [10] Wörner *et al* H J 2011 *Science* **334** 208
- [11] Lewenstein M, Balcou P, Ivanov M Y, L'Huillier A and Corkum P B 1994 *Phys. Rev. A* **49** 2117
- [12] Sheehy B, Martin J D D, DiMauro L F, Agostini P, Schafer K J, Gaarde M B and Kulander K C 1999 *Phys. Rev. Lett.* **83** 5270
- [13] Shan B and Chang Z 2001 *Phys. Rev. A* **65** 011804
- [14] Tate J, Auguste T, Muller H G, Salières P, Agostini P and DiMauro L F 2007 *Phys. Rev. Lett.* **98** 013901
- [15] Shiner A D, Trallero-Herrero C, Kajumba N, Bandulet H-C, Comtois D, Légaré F, Giguere M, Kieffer J-C, Corkum P B and Villeneuve D M 2009 *Phys. Rev. Lett.* **103** 073902
- [16] Le A-T, Lucchese R R, Tonzani S, Morishita T and Lin C D 2009 *Phys. Rev.* **80** 013401
- [17] Le A-T, Morishita T and Lin C D 2008 *Phys. Rev. A* **78** 023814
- [18] Frolov M V, Manakov N L, Sarantseva T S, Emelin M Y, Ryabikin M Y and Starace A F 2009 *Phys. Rev. Lett.* **102** 243901
- [19] Landau L D and Lifshitz E M 1977 *Quantum Mechanics: Non-Relativistic Theory (Course of Theoretical Physics vol 3)* 3rd edn (New York: Pergamon)
- [20] Cooper J W 1962 *Phys. Rev.* **128** 681
- [21] Wörner H J, Niikura H, Bertrand J B, Corkum P B and Villeneuve D M 2009 *Phys. Rev. Lett.* **102** 103901
- [22] Farrell J P, Spector L S, McFarland B K, Bucksbaum P H, Gühr M, Gaarde M B and Schafer K J 2011 *Phys. Rev. A* **83** 023420
- [23] Colosimo P *et al* 2008 *Nat. Phys.* **4** 386
- [24] Takahashi E J, Kanai T, Nabekawa Y and Midorikawa K 2008 *Appl. Phys. Lett.* **93** 041111
- [25] Schmidt B E *et al* 2010 *Appl. Phys. Lett.* **96** 121109
- [26] Hauri C P *et al* 2007 *Opt. Lett.* **32** 868
- [27] Vozzi C, Calegari F, Benedetti E, Gasilov S, Sansone G, Cerullo G, Nisoli M, Silvestri S D and Stagira S 2007 *Opt. Lett.* **32** 2957
- [28] Gu X *et al* 2009 *Opt. Express* **17** 62
- [29] Mücke O D, Ališauskas S, Verhoef A J, Pugžlys A, Baltuška A, Smilgevičius V, Pocius J, Giniūnas L, Danielius R and Forget N. 2009 *Opt. Lett.* **34** 2498
- [30] Béjot P, Schmidt B E, Kasparian J, Wolf J-P and Legaré F 2010 *Phys. Rev. A* **81** 063828
- [31] Trebino R, Delong K W, Fittinghoff D N, Sweetser J N, Krumbügel M A, Richman B A and Kane D J 1997 *Rev. Sci. Instrum.* **68** 3277
- [32] Huang K N, Johnson W R and Cheng K T 1981 *At. Data Nucl. Data Tables* **26** 33
- [33] Starace A F 1982 Theory of atomic photoionization *Handbuch der Physik*, vol 31 (Berlin: Springer) pp 1–121
- [34] Ganas P S and Green A E S 1971 *Phys. Rev. A* **4** 182
- [35] Schmidt M W *et al* 1993 *J. Comput. Chem.* **14** 1347